universe

MDPI

Article

Puzzling Low-Temperature Behavior of the Van Der Waals Friction Force between Metallic Plates in Relative Motion

George Dedkov

Nanoscale Physics Group, Kabardino-Balkarian State University, 360004 Nalchik, Russia; gv_dedkov@mail.ru

Abstract: This paper presents the results of calculating the van der Waals friction force (dissipative fluctuation-electromagnetic force) between metallic (Au) plates in relative motion at temperatures close to 1 K. The stopping tangential force arises between moving plates along with the usual Casimir force of attraction, which has been routinely measured with high precision over the past two decades. At room temperatures, the former force is 10 orders of magnitude less than the latter, but at temperatures $T < 50$ K, friction increases sharply. The calculations have been carried out in the framework of the Levin-Polevoi-Rytov fluctuation electromagnetic theory. For metallic plates with perfect crystal lattices and without defects, van der Waals friction force is shown to increase with decreasing temperature as T^{-4}. In the presence of residual resistance ρ_0 of the metal, a plateau is formed on the temperature dependence of the friction force at $T \to 0$ with a height proportional to ${\rho_0}^{-0.8}$. Another important finding is the weak force-distance dependence $\sim a^{-q}$ (with $q < 1$). The absolute values of the friction forces are achievable for measurements in AFM-based experiments.

Keywords: van der Waals friction force; Casimir force; Levin-Polevoi-Rytov fluctuation-electromagnetic theory; Drude model; low-temperature dependence

Citation: Dedkov, G. Puzzling Low-Temperature Behavior of the Van Der Waals Friction Force between Metallic Plates in Relative Motion. *Universe* **2021**, *7*, 427. https://doi.org/10.3390/universe7110427

Academic Editor: Galina L. Klimchitskaya

Received: 12 October 2021
Accepted: 5 November 2021
Published: 9 November 2021

1. Introduction

Spatial correlations of quantum and thermal fluctuations of polarization and magnetization of condensed bodies, as well as a vacuum electromagnetic field, lead to the appearance of fluctuating electromagnetic forces between polarizable particles, atoms, and macroscopic bodies. In particular, an attractive force arises between electrically neutral thick metallic or dielectric plates (half-spaces) located at a distance a from each other—the Casimir-Lifshitz force [1,2]. Fluctuation-electromagnetic forces in various systems are usually called van der Waals forces [3]. Upon the relative motion of the plates with velocity V, in addition to an attractive force, a dissipative tangential force (quantum friction force at $T = 0$) arises between them [4–16]. At nonrelativistic velocities V and temperature $T \neq 0$, this force is proportional to V and to higher odd powers of V^- at $T = 0$.

For several decades, the calculation of the van der Waals dissipative force has been the subject of intense theoretical research and discussion by numerous groups of authors, with widely differing results. In particular, the expressions for this force, obtained in the first works [4–7], were considered either inaccurate or lacked sufficient details, while correct expressions, in the cases $T = 0$ and $T \neq 0$, were first obtained in [8–10]. However, as has recently been shown [17], basic results obtained earlier by Polevoi (Equations (1)–(4) in [6]) make it possible to correctly reproduce all generally accepted expressions for the dissipative van der Waals force between parallel plates. In addition, a more transparent formula for this force, obtained on the basis of these results in [17], makes it possible to significantly simplify the analysis of its low-temperature dependence. As we have noted in [17], dissipative tangential force F_x between metallic (Au) plates increases sharply with decreasing temperature and decreasing electrical resistance. This unexpected result is associated with a significant increase of the contribution from low-frequency electromagnetic modes with frequencies $\omega \ll \nu$, with ν being the relaxation frequency, which, although small, is finite at $T = 0$. At the same time, at $\nu = 0$, the force F_x becomes negligibly small.

Along with these results, a general consensus has emerged between several theoretical approaches to the problem of dissipative van der Waals interactions on the whole, reflected, for example, in [11,18–20]. These developments and the results obtained and shown below open up much more optimistic prospects for conducting appropriate experiments to measure van der Waals friction, despite its smallness at ordinary (room) temperatures that hampers experimental studies.

Unlike dissipative van der Waals forces, precise experimental measurements of attractive Casimir-Lifshitz force F_z have been carried out for more than 20 years [21–23], having achieved a high accuracy of $\sim 1\%$, but at temperatures of ~ 1 K, thermal corrections to F_z are small compared to a "cold" part. This fact greatly complicates experimental measurements of entropy and, accordingly, the resolution of another long-standing problem—-the so-called Casimir puzzle and Casimir conundrum [23–26] in the case of metallic and dielectric plates: violating the Nernst heat theorem when calculating the force of attraction between the plates in the framework of the Lifshitz theory using conventional, well-tested dielectric functions of materials. A recent comprehensive review on this issue is given in [27]. In contrast, the van der Waals friction force with a linear dependence on velocity turns out to be most sensitive precisely to the low-temperature dielectric properties of materials, and its measurement can also give a new impetus in solving the Casimir puzzle.

In addition to fundamental interest, exploring van der Waals friction can be of great practical importance for microtechnology and for description of micromechanical systems operation [28]. There is also reason to guess that van der Waals friction can manifest itself under astrophysical conditions during conglomeration of dust particles [19,29].

Taking all the above into account, this work aims at a more detailed analytic and numerical analysis of the low-temperature behavior of the van der Waals friction force between metallic plates, based on the theory by Levin-Polevoi-Rytov [6,30] and its development in [17]. This enables us to confirm our previous conclusions [17] both analytically and numerically. Namely, van der Waals friction force between the plates of gold increases by 6–7 orders of magnitude when the temperature drops down from 100 to 1 K, provided that the dielectric permittivity is described by the Drude function, with the temperature dependence of relaxation frequency obeying the Bloch-Grüneisen formula or close to it. A simple analytic expression for the friction force is also obtained, and the conditions are discussed for its experimental measurement in the sphere-plate configuration, commonly used when measuring attractive Casimir force. This creates a favorable prospect in measuring van der Waals dissipative friction.

2. Theoretical Background

Let us consider the standard Casimir-Lifshitz configuration of a system of two metallic plates 1 and 2 (Figure 1) at a temperature T, separated by a vacuum gap a, where plate 1 moves with a nonrelativistic velocity V relative to a fixed plate 2. Recall the original expression for the fluctuation-electromagnetic friction force F_x per unit area of the vacuum contact of two plates obtained in [17] in a linear approximation in the velocity V (a more general formula is also given in [17]).

$$F_x = \frac{\hbar V}{2\pi^2}\int\limits_0^\infty d\omega \frac{dn}{d\omega}\int\limits_0^\infty dk k^3 \left[\frac{|q|^2}{|Q_e|^2}\mathrm{Im}\left(\frac{q_1}{\varepsilon_1}\right)\mathrm{Im}\left(\frac{q_2}{\varepsilon_2}\right)+\frac{|q|^2}{|Q_m|^2}\mathrm{Im}\left(\frac{q_1}{\mu_1}\right)\mathrm{Im}\left(\frac{q_2}{\mu_2}\right)\right], \quad (1)$$

where $n(\omega) = 1/(\exp(\hbar\omega/T)-1)$; $\varepsilon_{1,2}$ and $\mu_{1,2}$ are the frequency-dependent dielectric permittivity and magnetic permeability of materials of plate 1 and 2,

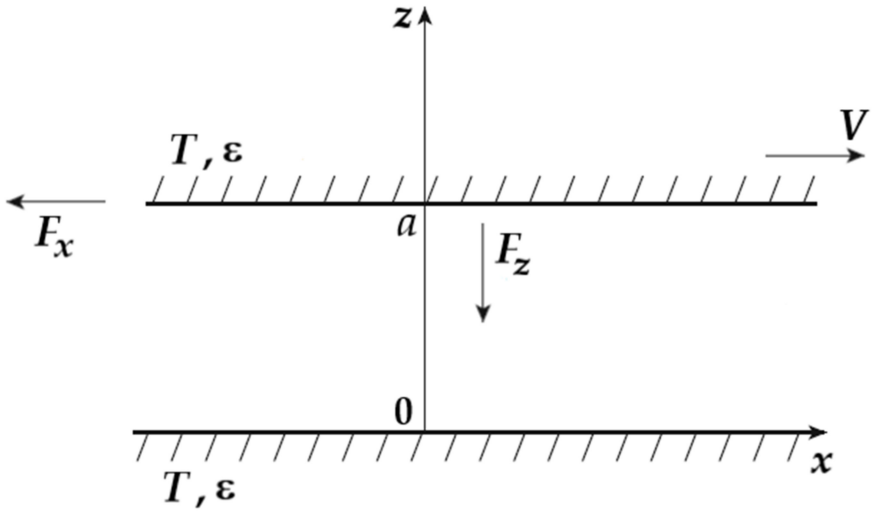

Figure 1. System configuration.

$q = \sqrt{k^2 - \omega^2/c^2}$, $q_{1,2} = \sqrt{k^2 - \varepsilon_{1,2}\mu_{1,2}\omega^2/c^2}$, and

$$Q_e = (q + q_1/\varepsilon_1)(q + q_2/\varepsilon_2)e^{qa} - (q - q_1/\varepsilon_1)(q - q_2/\varepsilon_2)e^{-qa}, \tag{2}$$

$$Q_m = (q + q_1/\mu_1)(q + q_2/\mu_2)e^{qa} - (q - q_1/\mu_1)(q - q_2/\mu_2)e^{-qa}. \tag{3}$$

In (1), the Planck constant and the speed of light in vacuum are denoted by $\hbar$ and c, and temperature T is expressed in energy units. The linear approximation in velocity corresponds to the condition $\omega \gg kV$, which at a nonrelativistic velocity $V \ll c$ is met both in the case of inhomogeneous (evanescent) electromagnetic waves ($k > \omega/c$) and in the case of propagating (traveling) waves ($k \leq \omega/c$). As shown in [17], formula (1) fully agrees with the general relativistic expression for the dissipative force F_x, obtained by Polevoi [6] within the framework of the fluctuation-electromagnetic theory [30]. It can also be cast to a more familiar expression with Fresnel's reflection coefficients of electromagnetic waves [10,11] (see Appendix A). However, formula (1) is much more convenient when analyzing the low-temperature behavior of the force F_x due to a more transparent dependence on dielectric permittivity.

We will further consider the case of plates of the same nonmagnetic metals with $\mu_1 = \mu_2 = 1$, $\varepsilon_1 = \varepsilon_2 = \varepsilon(\omega)$. Then (1) takes the simpler form

$$F_x = -\frac{\hbar V}{8\pi^2}\left(\frac{\hbar}{T}\right)\int_0^\infty \frac{d\omega}{\sin h^2(\hbar\omega/2T)}\int_0^\infty dk k^3|q|^2\left[\frac{\mathrm{Im}(q_1/\varepsilon)^2}{|Q_e|^2} + \frac{\mathrm{Im}(q_1)^2}{|Q_m|^2}\right]. \tag{4}$$

In obtaining (4), we have taken into account the identity $\frac{d}{dx}(\exp(x) - 1)^{-1} = -1/4\sin h^2(x/2)$. The modification of (2) and (3) for $\mu_1 = \mu_2$, $\varepsilon_1 = \varepsilon_2 = \varepsilon$ is obvious (keeping the general definition $q_1 = \sqrt{k^2 - \varepsilon\,\omega^2/c^2}$ for $q_{1,2}$).

When studying the low-temperature behavior of the attractive Casimir-Lifshitz force F_z between metallic plates, the Drude approximation for $\varepsilon(\omega)$ is usually used:

$$\varepsilon(\omega) = 1 - \frac{\omega_p^2}{\omega(\omega + i\nu)} \tag{5}$$

where ω_p and ν are plasma and relaxation frequencies. Meanwhile, for an ideal metal without impurities and other defects, dependence $\nu(T)$ obeys the Bloch-Grüneisen law [31,32].

$$\nu_{BG}(T) = 0.0212(T/\theta)^5\int_0^{\theta/T} x^5 \mathrm{sh}(x/2)^{-2}dx\ (\mathrm{eV}), \tag{6}$$

where θ is the Debye temperature. In the presence of impurities and other physical defects that contribute to the formation of residual resistance, it seems natural to use the expression

$$\nu(T) = \nu_0 + \nu_{BG}(T), \tag{7}$$

with ν_0 being the constant and $\nu_{BG}(T) \ll \nu_0$ at $0 \leq T \ll T_0$ ($T_0 \ll \theta$). The role of the relaxation frequency at zero temperature and the corresponding mechanisms were discussed in [32–36].

As can be easily seen from (4), only traveling waves $\omega/c \geq k$ can contribute to the friction force F_x at $\nu = 0$. The resulting friction force F_x in this case is extremely small for measurement at present. Therefore, direct experimental measurements of F_x at small distances between the plates, when inhomogeneous waves $k > \omega/c$ dominate, would not only be a direct validation of the presence of finite residual resistance but would also enable us to quantitatively assess its magnitude. In view of the above, we will further assume that function $\nu(T)$ is always nonzero and introduce the frequency parameterization $\omega = \nu t$. For wave vector k, we use the parametrization $k = (\omega_p/c)\sqrt{y^2 + \beta^2 t^2}$ (with $\beta = \nu/\omega_p$) in the case $k > \omega/c$, and $k = (\omega_p/c)\sqrt{\beta^2 t^2 - y^2}$ in the case $k \leq \omega/c$. Then, for q and q_1 in (4), we obtain $q = (\omega_p/c)y$, $q_1 = (\omega_p/c)\sqrt{y^2 + t/(t+\mathrm{i})}$ in the former case and $q = \mathrm{i}(\omega_p/c)y$, $q_1 = (\omega_p/c)\sqrt{-y^2 + t/(t+\mathrm{i})}$ in the latter case. Accordingly, formula (4) takes the form

$$F_x = -\frac{\hbar V}{8\pi^2}\left(\frac{\omega_p}{c}\right)^4 \alpha \int\limits_0^\infty \frac{dt}{\sinh^2(\alpha t/2)}[f_1(t,\beta,\lambda) + f_2(t,\beta,\lambda)], \tag{8}$$

where $\alpha = \hbar\nu/T$, $\lambda = \omega_p a/c$, and functions $f_{1,2}$ are given by

$$f_1(t,\beta,\lambda) = \int\limits_0^\infty dy y^2\left(y^2 + \beta^2 t^2\right)\left[\frac{(\mathrm{Im}(w_1/\epsilon))^2}{|Q_{en}|^2} + \frac{(\mathrm{Im} w_1)^2}{|Q_{mn}|^2}\right], \tag{9}$$

$$f_2(t,\beta,\lambda) = \int_0^{\beta t} dy y^2\left(\beta^2 t^2 - y^2\right)\left[\frac{(\mathrm{Im}(w_2/\epsilon))^2}{|Q_{er}|^2} + \frac{(\mathrm{Im} w_2)^2}{|Q_{mr}|^2}\right]. \tag{10}$$

In (9) and (10), we also introduced the quantities $\epsilon = 1 - 1/\left(\beta^2 t(t+\mathrm{i})\right)$, $w_1 = \sqrt{y^2 + t/(t+\mathrm{i})}$, $w_2 = \sqrt{-y^2 + t/(t+\mathrm{i})}$ and

$$Q_{mn} = 2\left(2y^2 + \frac{t}{t+\mathrm{i}}\right)\mathrm{sh}(\lambda y) + 4y\sqrt{y^2 + \frac{t}{t+\mathrm{i}}}\,\mathrm{ch}(\lambda y), \tag{11}$$

$$Q_{en} = 2\left(y^2 + \epsilon^{-2}\left(y^2 + \frac{t}{t+\mathrm{i}}\right)\right)\mathrm{sh}(\lambda y) + 4y\epsilon^{-1}\sqrt{y^2 + \frac{t}{t+\mathrm{i}}}\,\mathrm{ch}(\lambda y), \tag{12}$$

$$Q_{mr} = 2\left(-2y^2 + \frac{t}{t+\mathrm{i}}\right)\sin(\lambda y) + 4y\sqrt{-y^2 + \frac{t}{t+\mathrm{i}}}\,\cos(\lambda y), \tag{13}$$

$$Q_{er} = 2\left(-y^2 + \epsilon^{-2}\left(-y^2 + \frac{t}{t+\mathrm{i}}\right)\right)\sin(\lambda y) + 4y\epsilon^{-1}\sqrt{-y^2 + \frac{t}{t+\mathrm{i}}}\,\cos(\lambda y). \tag{14}$$

Let us analyze the role of individual terms in (8) as $T \to 0$, when the parameter $\alpha = \hbar\nu(T)/T$ is small. If $\nu(T)$ is defined by (6), then $\alpha = 1$ for $T = 69$ K and $\alpha = 1.375$ for $T = 300$ K. Moreover, up to high temperatures $T \sim 1000$ K, the relation $\alpha/\beta = \hbar\omega_p/T \gg 1$ holds. Parameter λ does not depend on temperature. In particular, for gold ($\omega_p = 9.03$ eV) at $a = 10$ nm, we obtain $\lambda = 0.459$. The presence of the hyperbolic sine squared in (8) enhances the role of low-frequency modes with $t \ll 1$, when $\mathrm{sh}(\alpha t/2)^{-2} \approx 4\alpha^{-2}t^{-2}$. Accordingly, a significant temperature effect should manifest itself at $T \ll 69$ K. To allocate

the dependence of the force F_x on α (and on temperature) more clearly, we write (8) in the form

$$F_x = -\frac{\hbar V}{8\pi^2}\left(\frac{\omega_p}{c}\right)^4 \frac{1}{\alpha}(I_{mn} + I_{en} + I_{mr} + I_{er}) \tag{15}$$

where the integral terms in square brackets are given by

$$I_{mn} = \alpha^2 \int_0^\infty \frac{dt}{\sin h^2(\alpha t/2)} \int_0^\infty dy y^2 \left(y^2 + \beta^2 t^2\right) \mathrm{Im}\left(\sqrt{y^2 + t/(t+\mathrm{i})}\right)^2 |Q_{mn}|^{-2}, \tag{16}$$

$$I_{en} = \alpha^2 \int_0^\infty \frac{dt}{\sin h^2(\alpha t/2)} \int_0^\infty dy y^2 \left(y^2 + \beta^2 t^2\right) \mathrm{Im}\left(\epsilon^{-1}\sqrt{y^2 + t/(t+\mathrm{i})}\right)^2 |Q_{en}|^{-2}, \tag{17}$$

$$I_{mr} = \alpha^2 \int_0^\infty \frac{dt}{\sin h^2(\alpha t/2)} \int_0^{\beta t} dy y^2 \left(\beta^2 t^2 - y^2\right) \mathrm{Im}\left(\sqrt{y^2 + t/(t+\mathrm{i})}\right)^2 |Q_{mr}|^{-2}, \tag{18}$$

$$I_{er} = \alpha^2 \int_0^\infty \frac{dt}{\sin h^2(\alpha t/2)} \int_0^{\beta t} dy y^2 \left(\beta^2 t^2 - y^2\right) \mathrm{Im}\left(\epsilon^{-1}\sqrt{y^2 + t/(t+\mathrm{i})}\right)^2 |Q_{er}|^{-2}. \tag{19}$$

The temperature dependence of F_x also manifests itself through a small parameter β. An analysis of (16)–(19) shows that, in the most important range of nanometer distances, a between the plates, the main contribution is made by the integral I_{mn}, corresponding to inhomogeneous waves. When calculating I_{mn}, y takes characteristic values $y \sim \lambda^{-1} \sim 1$. Then for $t \ll 1$ and $y \gg t$, one obtains $|Q_{mn}|^2 \approx 16y^4 \exp(2\lambda y)$. On the other hand, regardless of the relation between y and t, it follows that

$$(\mathrm{Im} w_1)^2 = \left(\mathrm{Im}\sqrt{y^2 + \frac{t}{t+\mathrm{i}}}\right)^2 = \frac{\sqrt{t^2 + [t^2 + y^2(1+t^2)]^2} - t^2 - y^2(1+t^2)}{2(1+t^2)}. \tag{20}$$

Accordingly, for $t \ll 1$ and $y \gg t$, one obtains $(\mathrm{Im} w_1)^2 \approx 0.5t^2/y^2(1+t^2)$ and $(\mathrm{Im} w_1)^2/|Q_{mn}|^2 \approx t^2 e^{-2\lambda y}/32y^6(1+t^2)$, while (16) takes the form

$$I_{mn} \approx \frac{1}{8}\int_0^p \frac{dt}{(1+t^2)} \int_p^\infty dy \frac{e^{-2\lambda y}}{y^2}\left(1 + \frac{\beta^2 t^2}{y^2}\right), \tag{21}$$

where $p \sim 1$. Calculating integral (17) yields,

$$I_{mn} = \frac{\mathrm{arctg} p}{8p}\left[2p\lambda \mathrm{Ei}(-2p\lambda) + e^{-2p\lambda}\right] + \frac{\beta^2}{24}\frac{(p - \mathrm{arctg} p)}{p^3}\left[4p^3\lambda^3 \mathrm{Ei}(-2p\lambda) + \left(1 - p\lambda + 2p^2\lambda^2\right)e^{-2p\lambda}\right] \tag{22}$$

with $\mathrm{Ei}(-x)$ being the integral exponential function [37]. Moreover, the presence of a small parameter β^2 in the second term of (22) makes it negligible in comparison with the first term. In the case when $y \ll t \ll 1$, from (11) and (20) it follows that $(\mathrm{Im} w_1)^2/|Q_{mn}|^2 \approx (1+y^2)/16y^2$, and when this expression is substituted into (16), the result does not depend on α, but it is negligible due to the smallness of the upper limits of integration. In other regions of integration, integral I_{mn} turns out to be proportional to α or α^2, so its contribution at $\alpha \ll 1$ can also be neglected. The rest of the integral terms in (15) are also small. In particular, integral I_{en} is cut off due to the large modulus value of the dielectric constant ε (ϵ in (9)), and the contributions I_{mr} and I_{er} from traveling waves are small due to the additional dependence on β^2. Thus, taking into account (18), it follows from (15) that at $T \to 0$ force, F_x increases proportionally to T^{-4} if $\nu(T)$ is described by (6). This conclusion is also confirmed by direct numerical calculations in Section 3.

3. Numerical Results

As an example, we calculated the van der Waals force between two Au plates. The dielectric function was taken in Drude approximation (5) with the relaxation frequency

defined by (6) or (7). When using (7), parameter ν_0 was varied in such a way that the equality $\nu_0 = \nu_{BG}(T_0)$ was fulfilled for values of T_0 in the range from 0 to 3 K. This made it possible to estimate the residual resistance of the plate material, $\rho_0 = 4\pi\nu_0/\omega_p^2$. Accordingly, parameter α in (15)–(19) was calculated by $\alpha(T) = (\nu_0 + \nu_{BG}(T))/T$. In Table 1, we compare different contributions to the friction force (I_{mn}, I_{en}, I_{mr}, I_{er}) in Equation (15). One can see that integrals I_{en}, I_{mr}, I_{er} are small compared to I_{mn} and can be neglected. The resultant friction forces at $\nu_0 = 0$ are shown in Table 2. The upper-row values of F_x for each temperature T and a gap width a were obtained by direct numerical integration of (16). The lower-row values of F_x were calculated by formula (22) with parameter p depending on a. Since the temperature dependence of integral I_{mn} was very weak, a good approximation for $p(a)$ at each value of a was obtained when equating (22) and the result of numerical integration in (16) for $T = 1$ K. The resultant dependence $p(a)$ is shown by the solid curve in Figure 2. The dashed curve was obtained using the fitting function

$$p(a) = 0.4 \exp\left(-0.1a^{1/2} - 0.001a^{0.874}\right). \quad (23)$$

Table 1. Integrals $I_{mn}, I_{en}, I_{mr}, I_{er}$.

		a=10 **nm**		
T K	I_{mn}	I_{en}	I_{mr}	I_{er}
1	8.08×10^4	4.91×10^{-34}	8.43×10^{-29}	8.94×10^{-29}
5	129.3	7.49×10^{-23}	4.12×10^{-21}	4.36×10^{-21}
10	8.087	4.84×10^{-18}	8.02×10^{-18}	8.89×10^{-18}
50	0.0785	1.46×10^{-9}	2.91×10^{-12}	3.77×10^{-12}
		$a = 50$ **nm**		
T K	I_{mn}	I_{en}	I_{mr}	I_{er}
1	3.031×10^4	9.77×10^{-35}	2.91×10^{-29}	7.14×10^{-29}
5	48.5	1.49×10^{-23}	1.42×10^{-21}	3.49×10^{-21}
10	3.031	9.77×10^{-19}	2.78×10^{-18}	7.1×10^{-18}
50	0.0296	6.54×10^{-11}	1.14×10^{-12}	3.07×10^{-12}

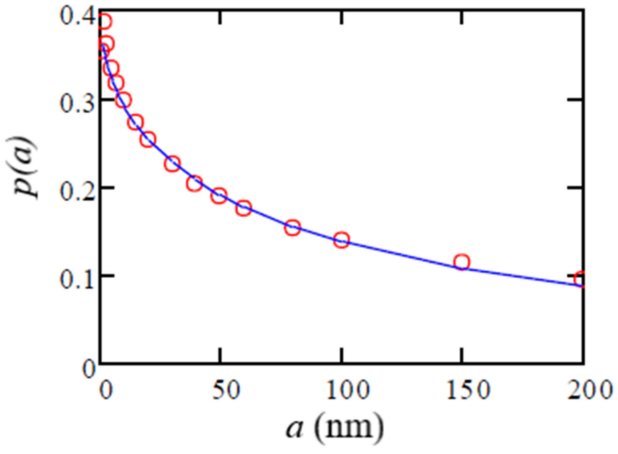

Figure 2. Dependence $p(a)$ in (22) (circles) as a function of the gap width a, obtained when equalizing (16) and (22) for $T = 1$ K and $\nu_0 = 0$ in (7). Solid line extrapolation (23).

Table 2. Van der Waals friction force between two Au plates (N/m^2), $V = 1$ m/s. The upper-rows of data correspond to Equation (15) with (16), while the lower-rows data correspond to Equation (24) with (23).

a, nm	T = 0.5 K	T = 1 K	T = 5 K	T = 10 K	T = 50 K
1	13.1	0.818	1.309×10^{-3}	8.18×10^{-5}	7.90×10^{-7}
	13.0	0.814	1.302×10^{-3}	8.14×10^{-5}	7.95×10^{-7}
5	9.55	0.597	9.55×10^{-4}	5.97×10^{-5}	5.78×10^{-7}
	9.72	0.608	9.72×10^{-4}	6.08×10^{-5}	5.94×10^{-7}
10	7.48	0.468	7.48×10^{-4}	4.68×10^{-5}	4.54×10^{-7}
	7.57	0.473	7.57×10^{-4}	4.73×10^{-5}	4.62×10^{-7}
20	5.29	0.330	5.29×10^{-4}	3.31×10^{-5}	3.22×10^{-7}
	5.24	0.328	5.24×10^{-4}	3.28×10^{-5}	3.20×10^{-7}
30	4.09	0.256	4.09×10^{-4}	2.56×10^{-5}	2.49×10^{-7}
	3.98	0.248	3.98×10^{-4}	2.49×10^{-5}	2.43×10^{-7}
40	3.33	0.208	3.33×10^{-4}	2.08×10^{-5}	2.03×10^{-7}
	3.18	0.198	3.18×10^{-4}	1.99×10^{-5}	1.94×10^{-7}
50	2.81	0.175	2.81×10^{-4}	1.75×10^{-5}	1.71×10^{-7}
	2.63	0.164	2.63×10^{-4}	1.64×10^{-5}	1.61×10^{-7}
100	1.55	0.0969	1.55×10^{-4}	9.69×10^{-6}	9.48×10^{-8}
	1.39	0.0868	1.39×10^{-4}	8.68×10^{-6}	8.48×10^{-8}
150	1.063	0.0665	1.063×10^{-4}	6.65×10^{-6}	6.53×10^{-8}
	0.965	0.0603	9.65×10^{-5}	6.03×10^{-6}	5.90×10^{-8}
200	0.404	0.0504	8.07×10^{-5}	5.05×10^{-6}	4.91×10^{-8}
	0.773	0.0483	7.73×10^{-5}	4.83×10^{-6}	4.72×10^{-8}

As follows from the data in Table 2, the use of (22) in combination with (23) provides a fair description of the friction force. Approximation errors gradually increase from 0–3% for $a \leq 30$ nm to 3–10% for $30 \leq a \leq 200$ nm. Errors are associated with increasing errors of Equation (23) at large values of a

Omitting the small second term in (22) and inserting (22) into (15), we obtain an approximate expression for the friction force of the form

$$F_x = -\frac{\hbar V}{64\pi^2}\left(\frac{\omega_p}{c}\right)^4 \frac{T}{\nu(T)} \frac{\mathrm{arctg}\, p}{p}\left[\frac{2p\omega_p a}{c}\mathrm{Ei}\left(-2p\omega_p a/c\right) + \exp\left(-2p\omega_p a/c\right)\right], \qquad (24)$$

where $p(a)$ is given by (23) or it can be taken from Figure 2 (circles) and Table 3.

Table 3. Function $p(a)$.

a, nm	1	2	3	5	7	10	15	20
$p(a)$	0.352	0.385	0.360	0.334	0.318	0.297	0.272	0.254
a	30	40	50	60	80	100	150	200
$p(a)$	0.225	0.204	0.188	0.175	0.154	0.139	0.113	0.0955

As follows from (24) and the data shown in Table 2, at $T \sim 1 - 200$ K, friction force F_x scales as T^{-4} if $\nu_0 = 0$. This is caused by dependence (6). Another striking result is that in the range of distances under consideration (see Figure 3).

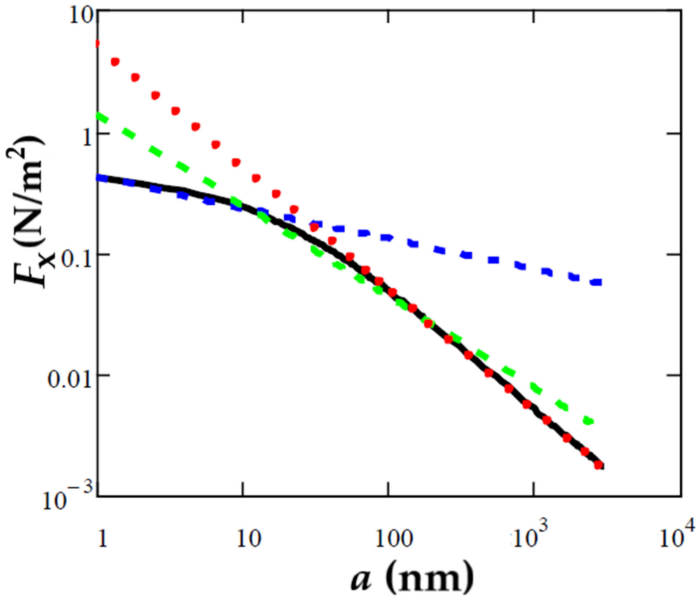

Figure 3. Friction force between two Au plates as a function of gap width a for $T = T_0 = 1$ K, $V = 1$ m/s. The black line shows the result of numerical calculation. The red, green, and blue lines correspond to analytic fits $5a^{-1}$, $1.37a^{-0.75}$, and $0.41a^{-0.25}$.

The dependence of F_x on distance (gap width) is relatively weak: $F_x(a) \sim a^{-0.25}$ for $a = 1 - 10$ nm, $F_x(a) \sim a^{-0.75}$ for $a = 10 - 100$ nm, and $F_x(a) \sim a^{-1}$ for $a = 100 - 3000$ nm. This is in drastic contrast to the behavior of the attractive Casimir force ($F_z \sim a^{-4}$ for $T = 0$ in this range of separations).

As the next step, we calculated dependence $F_x(T)$ at different values of ν_0. The results are shown in Figures 4 and 5 for $a = 10$ nm and $a = 100$ nm.

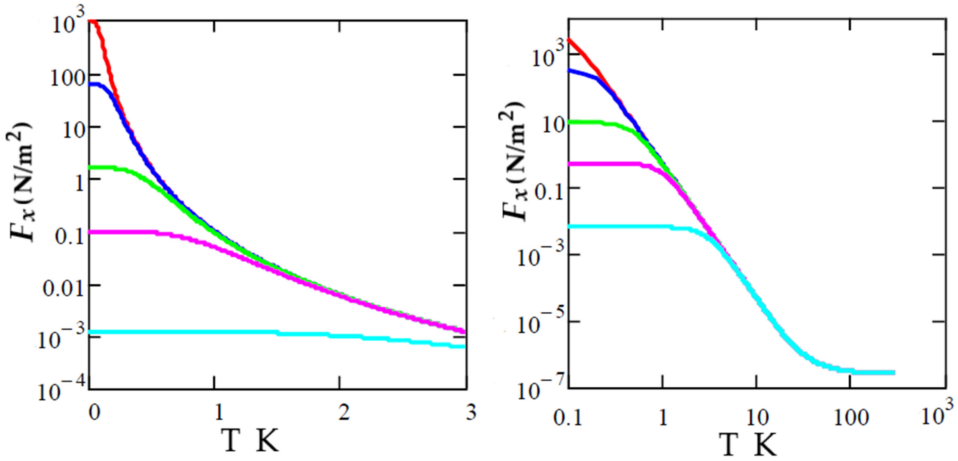

Figure 4. Friction force between Au plates as a function of temperature T and parameter T_0 for a gap width $a = 10$ nm and $V = 1$ m/s. The top (red) to bottom (light blue) curves correspond to $T_0 = 0.1,\ 0.2,\ 0.5,\ 1,\ 3$ K, respectively.

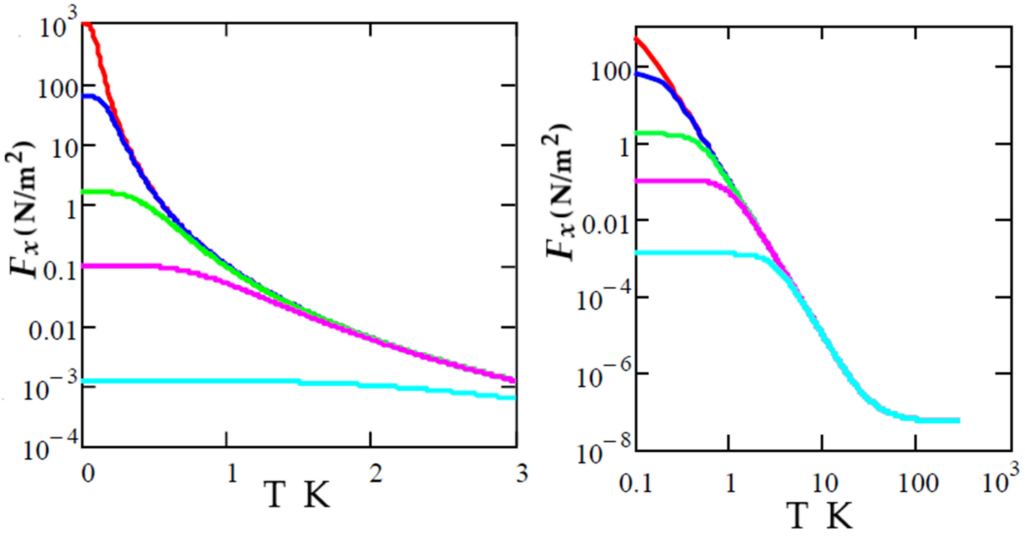

Figure 5. Friction force between Au plates as a function of temperature T and parameter T_0 for a gap width $a = 100$ nm and $V = 1$ m/s. The top (red) to bottom (light blue) curves correspond to $T_0 = 0.1,\ 0.2,\ 0.5,\ 1,\ 3$ K, respectively.

The formation of a plateau on the plots at $T = 0$ was caused by the finite values of ν_0 and residual resistance ρ_0. The smaller ν_0, the higher the growth of $F_x(T)$ with decreasing temperature. A plateau was formed at a temperature T_0, corresponding to the equality $\nu_0 = \nu_{BG}(T_0)$, and the corresponding values of F_x were proportional to $\rho_0^{-0.8}$. Another plateau on the curves, where the friction force barely does not depend on temperature, was observed at $T > 100$ K, in the range of room and higher temperatures, in agreement with our previous calculations [17].

4. Discussion

The results obtained fully confirm our earlier conclusion [17] that van der Waals friction force between metallic plates of gold should increase significantly at temperatures $T < 50$ K (see Figures 4 and 5). The character of this dependence ($F_x \sim T^{-4}$) is due to the low-temperature behavior of the relaxation frequency $\nu(T)$ at $T < \theta$, since $\nu(T) \sim T^5$. In the presence of defects and impurities in the metal, the quantity $\nu(0) = \nu_0$ is associated with the residual resistance of the metal, $\rho_0 = 4\pi\nu_0/\omega_p^2$. With decreasing temperature below the value T_0 determined by the relation $\nu_{BG}(T_0) = \nu_0$, the height of the plateau forming on the dependence of the friction force on temperature is proportional to T_0^{-4}. Correspondingly, knowing the height of the plateau allows one to find ρ_0, since $F_x \propto \rho_0^{-0.8}$. At first glance, an unexpected increase in friction at $T < 100$ K (69 K for gold) had a fairly simple physical justification. In accordance with the Planck distribution, the density of fluctuation modes increased significantly at low frequencies $\omega < T/\hbar$. However, under normal conditions and a sufficiently high resistance of the metal, the relationship $\nu > T/\hbar$ ($\alpha > 1$) was satisfied, and the characteristic absorption frequency was the Wien frequency. Accordingly, friction force decreased with decreasing temperature ($\propto T^2$). With decreasing temperature T, the relaxation frequency decreased faster than the Wien frequency, the ratio between them changed ($\alpha < 1$), and the characteristic absorption frequency shifted towards low frequencies with a high density of electromagnetic modes. At the same time, the penetration depth of S-modes increased. Although the mean free path of electrons increased and the resistance to direct current dropped down, an increasing number of electrons underwent small-angle scattering under the action of numerous small-scale local fluctuations of the electromagnetic field and charge density. As a result, Joule dissipation and friction grew up to the saturation threshold due to residual resistance. In general, these processes were controlled by parameter α. Within the framework of this scheme, the sharp drop in the friction force in the limit $T \to 0$, $\nu \to 0$ is also easily explained: the S-wave field was

transformed into a constant magnetic field that freely penetrated into the sample, and the dissipation of energy of electrons disappeared.

Thus, no less important result is that the dominant contribution to the friction force (up to distances $a = 1 \div 3$ μm) was due to inhomogeneous S-polarized electromagnetic waves. Meanwhile, it was the low-temperature behavior of the S-modes and their contribution to the magnitude of the thermal part of the Casimir force that played a key role in resolving the Casimir paradox associated with a possible violation of the Nernst theorem, since theoretically consistent models of dielectric response for real metals at low frequencies should agree with the behavior of the Casimir entropy at $T \to 0$. According to [32], the most promising route for exploring the finite temperature correction to the Casimir pressure and entropy in the standard setup with two parallel plates appears to be the case of large separations around 2 μm. Then the corresponding (relative) temperature correction will be on the level of 1%. However, at such separations, the Casimir pressure itself is small (it is $\sim 1.6 \times 10^4$ times less than at separations of 100 nm). At the same time, if van der Waals friction increases by $10^6 \div 10^8$ times at $T \sim 1$ K, the level of thermal correction to Casimir pressure will be inferior to the magnitude of the van der Waals friction. For ideal metal plates, at $a = 2$ μm, $T = 3$ K, the thermal Casimir force $F_z = -1.2T/4\pi a^3$ turns out to be 5×10^{-7} N/m^2, whereas the corresponding friction force was 3.2×10^{-5} N/m^2 (at $V = 1$ m/s, $T = T_0 = 3$ K), i.e., much higher.

Also noteworthy was the very slow decrease in the friction force with distance: even at $a = 1 \div 3$ μm we obtained the dependence $F_x \sim a^{-1}$, while at smaller distances we had $F_x \sim a^{-q}$ with $q < 1$ (Figure 3). This is in drastic contrast to the Casimir attraction force, where $F_z \sim a^{-q}$ with $q = 4 \div 3$. Such a weak dependence lead to an increase in the effective area of interaction in experiments, in which a probing body was a metallized sphere of radius R. In addition, the role of surface roughness in this case also turned out to be less important.

The calculated values of the van der Waals friction force seem to be quite achievable in a setup based on an atomic force microscope (AFM), where an Au-coated sphere of radius R is attached to the AFM cantilever and interacts with an Au-coated plate of the substrate material. Thus, for $R = 50$ μm, $a = 20$ nm, $T = T_0 = 1$ K, and $V = 1$ m/s, we obtained $F_x = 0.165$ N/m^2 and $F_x = 0.088$ N/m^2 (at $a = 50$ nm and the same other conditions). Then, with an effective area of interaction $S_{eff} = \pi a R$, the calculated friction parameter will be $\gamma = F_x S_{eff}/V = 5.2 \times 10^{-13}$ kg/s in the former case and $\gamma = 6.9 \times 10^{-13}$ kg/s in the latter. Close to such experimental conditions were those implemented in [38]. In that experiment, a configuration with the AFM cantilever oriented perpendicular to the surface was applied. Due to the high stiffness of the cantilever in the transverse direction, the distance a between the sphere and the surface could be controlled with an accuracy of several nm. The measured values of the friction parameter γ (at $a = 10$ nm) were 1.5×10^{-13} kg/s at $T = 295$ K and 2.5×10^{-14} kg/s at $T = 77$ K, with the distance dependence $\gamma \sim a^{-q}$ ($q = 1.3 \pm 0.2$). However, the dissipation mechanism in [38] was not clearly elucidated. However, in the opinion of the authors, the dissipation is electrical in origin, and they did not exclude the influence of adsorbates and other surface defects, causing the appearance of parasitic electric fields. To a greater extent, such effects were likely even more significant in the experiment [39], with a parallel orientation of the cantilever (in the range of room temperatures). As compared to our expectations, the key points, which likely exclude the relevance of these experiments to the quantitative estimates of the van der Waals friction, are related with the decreasing temperature dependence (with reducing temperature). In addition, the level of the van der Waals friction of order 10^{-13} kg/s is expected at temperatures $T < 5$ K, which were not reached in [34].

New fascinating experimental possibilities in precision measurements of Casimir forces and quantum friction forces between plates and in close geometry are opening up with recent experiments [36,40,41]. In particular, in [41], the Casimir force between interpenetrated rectangular gratings was measured at $T = 4$ K.

Another point that seems to be worth touching on briefly is the possible role of nonlocal corrections to the dielectric constant at low temperatures. In our recent paper [42], the calculated nonlocal correction to friction force becomes significant at separations $a < 10$ nm, but it affects only the contribution from P-polarized waves, which is much less than the contribution from S-waves (Table 1). In addition, this nonlocal correction scales with temperature and distance as T^2/a^5. The effect of nonlocality was also negligible in calculating the contribution from S-waves to Casimir pressure [43,44]. One more nonlocal modification of Drude function (5) (compared to [43,44]) was recently proposed in [45]. In its essential point, as far as concerned the friction force, the second term in (5) had an additional factor $\sim 1/(1+\mathrm{i}kV_F/\omega)$. In the case of interest, $k > \omega/c$, this factor either did not change the Drude-like low-temperature behavior of dielectric permittivity, $\varepsilon \approx \mathrm{i}\omega_p^2/\omega\nu(T)$ ($\omega \ll \nu(T)$) or lead to the plasma-like dependence. In the latter case, the friction force receded. A more confident judgement needs additional analysis.

5. Conclusions

The main conclusions are the following:

(1) For metals without defects and impurities, van der Waals friction parameter $\gamma = F_x/V$ increases with decreasing temperature as T^{-4} at temperatures $T < 100$ K.
(2) In the presence of residual resistance ρ_0, the temperature dependence of the friction force reaches saturation ($\gamma \propto \rho_0^{-0.8}$) at $T < T_0$, where T_0 depends on the magnitude of ρ_0.
(3) Dependence of the friction parameter on distance is weak: $\gamma \sim a^{-q}$ with $q \leq 1$ up to $a = 3$ μm.
(4) Absolute values of van der Waals friction at $T < 1 \div 5$ K are large enough to be measured with existing AFM techniques.

Funding: This research received no external funding.

Institutional Review Board Statement: Not applicable.

Informed Consent Statement: Not applicable.

Data Availability Statement: All necessary data are contained in this article.

Acknowledgments: The author is grateful to I.H. Brevik for the useful information and comments.

Conflicts of Interest: The author declares no conflict of interest.

Appendix A

As shown in [17], the following identities take place

$$\mathrm{Im}(q_1/\varepsilon_1)\mathrm{Im}(q_2/\varepsilon_2) = \begin{cases} -\frac{\mathrm{Im}\Delta_{1e}\mathrm{Im}\Delta_{2e}}{|q|^2|\varepsilon_1|^2|\varepsilon_2|^2}|\varepsilon_1 q + q_1|^2|\varepsilon_2 q + q_2|^2, & k > \omega/c \\ -\frac{1}{4}\frac{(1-|\Delta_{1e}|^2)(1-|\Delta_{2e}|^2)}{|q|^2|\varepsilon_1|^2|\varepsilon_2|^2}|\varepsilon_1 q + q_1|^2|\varepsilon_2 q + q_2|^2, & k \leq \omega/c \end{cases}, \quad \text{(A1)}$$

$$\mathrm{Im}(q_1)\mathrm{Im}(q_2) = \begin{cases} -\frac{\mathrm{Im}\Delta_{1m}\mathrm{Im}\Delta_{2m}}{|q|^2}|q + q_1|^2|q + q_2|^2, & k > \omega/c \\ -\frac{1}{4}\frac{(1-|\Delta_{1m}|^2)(1-|\Delta_{2m}|^2)}{|q|^2}|q + q_1|^2|q + q_2|^2, & k \leq \omega/c \end{cases}, \quad \text{(A2)}$$

$$|Q_\varepsilon|^2 = |\varepsilon_1 q + q_1|^2|\varepsilon_2 q + q_2|^2\left|1 - \Delta_{1e}\Delta_{2e}e^{-2qa}\right||\varepsilon_1|^2|\varepsilon_2|^2\left|e^{2qa}\right|, \quad \text{(A3)}$$

$$\left|Q_\mu\right|^2 = |q + q_1|^2|q + q_2|^2\left|1 - \Delta_{1m}\Delta_{2m}e^{-2qa}\right|\left|e^{2qa}\right|, \quad \text{(A4)}$$

where $\Delta_{ie} = \frac{\varepsilon_i q - q_i}{\varepsilon_i q + q_i}$ and $\Delta_{im} = \frac{q - q_i}{q + q_i}$ are the reflection coefficients for the P-polarized and S-polarized electromagnetic waves (i = 1,2), $q = \sqrt{k^2 - \omega^2/c^2} = |q|$ for $k > \omega/c$ and $q = \mathrm{i}|q|$ for $k \leq \omega/c$. Inserting (A1)–(A4) into (1) we obtain

$$F_x = \frac{\hbar V}{2\pi^2}\int\limits_0^\infty \left(\frac{\partial n}{\partial \omega}\right) d\omega \int\limits_{\omega/c}^\infty dk k^3 e^{-2qa}\mathrm{Im}\Delta_{1e}\mathrm{Im}\Delta_{2e}|D_e|^{-2} + \frac{\hbar V}{8\pi^3}\int\limits_0^\infty \left(\frac{\partial n}{\partial \omega}\right) d\omega \int\limits_0^{\omega/c} dk k^3 \left(1-|\Delta_{1m}|^2\right)\left(1-|\Delta_{2m}|^2\right)|D_e|^{-2} + (e \leftrightarrow m) \quad \text{(A5)}$$

where $D_e = 1 - \Delta_{1e}\Delta_{2e}e^{-2qa}$. Formula (A5) has become more familiar since works [10,11]. In the case $\mu_1 = \mu_2 = 1$, $\varepsilon_1 = \varepsilon_2 = \varepsilon$, using (A1)–(A4), we retrieve (A5).

References

1. Casimir, H.B.G. On the attraction between two perfectly conducting plates. *Proc. Kon. Ned. Akad. Wet. B* **1948**, *51*, 793–795.
2. Lifshitz, E.M. The theory of molecular attractive forces between solids. *Sov. Phys. JETP* **1956**, *2*, 73–83.
3. Barash, Y.S. *Van Der Waals Forces*; Nauka: Moscow, Russia, 1988. (In Russian)
4. Teodorovich, E.V. On the contribution of macroscopic van der Waals interactions to frictional force. *Proc. R. Soc.* **1978**, *A 362*, 71–77.
5. Levitov, L.S. Van der Waals friction. *Eur. Phys. Lett.* **1989**, *8*, 499–504. [CrossRef]
6. Polevoi, V.G. Tangential molecular forces between moving bodies by a fluctuating electromagnetic field. *Sov. Phys. JETP* **1990**, *71*, 1119–1124.
7. Mkrtchian, V.E. Interaction between moving macroscopic bodies: Viscosity of electromagnetic vacuum. *Phys. Lett. A* **1995**, *209*, 299–302. [CrossRef]
8. Pendry, J.B. Shearing the vacuum—Quantum friction. *J. Phys. C Condens. Matter* **1997**, *9*, 10301–10320. [CrossRef]
9. Kardar, M.; Golestanian, R. The friction of vacuum and other fluctuation-induced forces. *Rev. Mod. Phys.* **1999**, *71*, 1233–1245. [CrossRef]
10. Volokitin, A.I.; Persson, B.N.J. Theory of friction: The contribution from fluctuating electromagnetic field. *J. Phys. Condens. Matter* **1999**, *9*, 345–359. [CrossRef]
11. Volokitin, A.I.; Persson, B.N.J. Near-field radiation heat transfer and noncontact friction. *Rev. Mod. Phys.* **2007**, *79*, 1291–1329. [CrossRef]
12. Philbin, T.G.; Leonhardt, U. No quantum friction between uniformly moving plates. *New J. Phys.* **2009**, *11*, 033035. [CrossRef]
13. Pendry, J.B. Quantum friction–fact or fiction? *New J. Phys.* **2010**, *12*, 033028. [CrossRef]
14. Barton, G. On van der Waals friction between half-spaces at low temperature. *J. Phys. Condens. Matter* **2011**, *23*, 335004. [CrossRef] [PubMed]
15. Høye, J.S.; Brevik, I.; Milton, K.A. Casimir friction force between polarizable media. *Eur. Phys. J.* **2012**, *D 66*, 149. [CrossRef]
16. Høye, J.S.; Brevik, I. Casimir friction at zero and finite temperatures. *Eur. Phys. J.* **2014**, *D 68*, 61. [CrossRef]
17. Dedkov, G.V.; Kyasov, A.A. Friction and radiative heat exchange in a system of two parallel plate moving sideways: Levin-Polevoi-Rytov theory revisited. *Chin. Phys.* **2018**, *56*, 3002–3011. [CrossRef]
18. Høye, J.S.; Brevik, I.; Milton, K.A. The reality of Casimir friction. *Symmetry* **2016**, *8*, 29–42.
19. Dedkov, G.V.; Kyasov, A.A. Fluctuation-electromagnetic interaction under dynamic and thermal nonequilibrium conditions. *Phys. Usp.* **2017**, *60*, 559. [CrossRef]
20. Pieplow, G.; Henkel, C. Fully covariant radiation force on a polarizable particle. *New J. Phys.* **2013**, *15*, 023027. [CrossRef]
21. Lamoreaux, S.K. Demonstration of the Casimir force in the 0.6 to 6 μm range. *Phys. Rev. Lett.* **1997**, *78*, 5. [CrossRef]
22. Mohideen, U.; Roy, A. Precision measurement of the Casimir force from 0.1 to 0.9 μm. *Phys. Rev. Lett.* **1998**, *81*, 4549. [CrossRef]
23. Klimchitskaya, G.L.; Mostepanenko, V.M. Experiment and theory in the Casimir effect. *Contemp. Phys.* **2006**, *47*, 131–144. [CrossRef]
24. Høye, J.S.; Brevik, I.; Milton, K.A. What is the temperature dependence of the Casimir effect? *J. Phys. Math. Gen.* **2006**, *39*, 6031–6038. [CrossRef]
25. Milton, K.A.; Li, Y.; Kalauni, P.; Parashar, P.; Guerodt, P.; Ingold, G.-L.; Lambrecht, A.; Reynaud, S. Negative entropies in Casimir and Casimir-Polder interactions. *Fortschr. Phys.* **2017**, *65*, 1600047. [CrossRef]
26. Bimonte, G.; Emig, T.; Kardar, M.; Kruger, M. Nonequilibrium fluctuational quantum electrodynamics: Heat radiation, heat transfer, and force. *Ann. Rev. Condens. Matter Phys.* **2017**, *8*, 119–143. [CrossRef]
27. Mostepanenko, V.M. Casimir puzzle and Casimir conundrum: Discovery and search for resolution. *Universe* **2021**, *7*, 84. [CrossRef]
28. Aspelmeyer, M.; Kippenberg, T.J.; Markuardt, F. Cavity optomechanics. *Rev. Mod. Phys.* **2014**, *86*, 1391–1455. [CrossRef]
29. Dedkov, G.V.; Kyasov, A.A. Dynamically and thermally nonequilibrium fluctuation-electromagnetic interactions: Recent results and trends. *Mod. Phys. Lett. A* **2020**, *35*, 2040013. [CrossRef]
30. Levin, M.L.; Polevoy, V.G.; Rytov, S.M. Contribution to the theory of heat exchange due to a fluctuating electromagnetic field. *Sov. Phys. JETP* **1980**, *52*, 1054–1063.
31. Condon, E.U.; Odishaw, H. *Handbook of Physics*, 2nd ed.; McGraw-Hill: New York, NY, USA, 1967.
32. Brevik, I.; Aarseth, J.B. Temperature dependence of the Casimir effect. *J. Phys. A Math. Gen.* **2006**, *39*, 6187–6193. [CrossRef]
33. Høye, J.S.; Brevik, I.; Aarseth, J.B.; Milton, K.A. Does the transverse electric zero mode contribute to the Casimir effect for a metal? *Phys. Rev. E* **2003**, *67*, 056116. [CrossRef]

34. Hoye, J.S.; Brevik, I.; Ellingsen, S.A.; Aaarseth, J.B. Analytical and numerical verification of the Nernst theorem for metals. *Phys. Rev. E* **2007**, *75*, 051127. [CrossRef] [PubMed]
35. Brevik, I.; Høye, J.S.; Ellingsen, S.A.; Milton, K.A. Analytical and numerical demonstration of how the Drude dispersive model satisfies Nernst's theorem for the Casimir entropy. *J. Phys. A Math.* **2008**, *41*, 164017. [CrossRef]
36. Bimonte, G.; Spreng, B.; Maia Neto, P.A.; Ingold, G.-I.; Klimchitskaya, G.L.; Mostepanenko, V.M.; Decca, R.S. Measurement of the Casimir Force between 0.2 and 8 μm: Experimental procedures and comparison with theory. *Universe* **2021**, *7*, 93. [CrossRef]
37. Gradshteyn, I.S.; Rhyzik, I.M. *Table of Integrals, Series, and Products*; Academic Press: New York, NY, USA, 2000.
38. Stipe, B.C.; Stowe, T.D.; Kenny, T.W.; Rugar, D. Noncontact friction and force fluctuations between closely spaced bodies. *Phys. Rev. Lett.* **2001**, *87*, 096801. [CrossRef] [PubMed]
39. Gotsmann, B.; Fuchs, H. Dynamic force spectroscopy of conservative and dissipative forces in an Al-Au (111) tip-sample contact. *Phys. Rev. Lett.* **2001**, *86*, 2597–2601. [CrossRef] [PubMed]
40. Farias, M.B.; Lombardo, F.C.; Alejandro Soba, A.; Villar, P.I.; Decca, R.S. Towards detecting traces of non-contact quantum friction in the corrections of the accumulated geometric phase. *NPJ Quantum Inf.* **2020**, *6*, 25. [CrossRef]
41. Wang, M.L.; Tang, L.; Ng, C.Y.; Messina, R.; Guizal, B.; Crosse, J.A.; Antezza, M.; Chan, C.T.; Ho Bun, C. Strong geometry dependence of the Casimir force between interpenetrated rectangular gratings. *Nat. Commun.* **2020**, *12*, 600. [CrossRef]
42. Dedkov, G.V.; Kyasov, A.A. Nonlocal friction forces in the particle-plate and plate-approximation: Nonretarded approximation. *Surf. Sci.* **2020**, *700*, 121681. [CrossRef]
43. Sernelius Bo, E. Effects of spatial dispersion on electromagnetic surface modes and on modes associated with a gap between two half spaces. *Phys. Rev. B* **2005**, *71*, 235114. [CrossRef]
44. Svetovoy, V.B.; Esquivel, R. Nonlocal impedances and the Casimir entropy at low temperatures. *Phys. Rev. E* **2005**, *72*, 036113. [CrossRef] [PubMed]
45. Klimchitskaya, G.L.; Mostepanenko, V.M. An alternative response to the off-shell quantum fluctuations: A step forward in resolution of the Casimir puzzle. *Eur. Phys. J. C* **2020**, *80*, 900. [CrossRef]